Computation of acoustic waves generated by a co-rotating vortex pair

K. Liow, M. C. Thompson and K. Hourigan

Department of Mechanical Engineering
Monash University, Victoria, 3800 AUSTRALIA

Abstract

The far field acoustic effects of a co-rotating vortex pair are modelled using Lighthill's [4] theory of turbulence-generated sound and Powell's [9] theory of vortex sound. To do this, the flow and acoustic fields are decoupled. The unsteady incompressible viscous flow field is modelled using conventional computational fluid dynamics techniques. The sound field is modelled separately using an inhomogeneous wave equation where the source is computed from the flow field variables. The robustness of the computational method in implementing Lighthill's [4] and Powells's [9] theories is demonstrated. The results are compared with those from direct numerical simulation (DNS) [7] and the analytical solution of [8]. It is found that by choosing an appropriate initial condition to the aeroacoustic governing equation, the levels of spurious waves are reduced quite dramatically.

Nomenclature

c	=	speed of sound in acoustic medium
CAA	=	Computational Aero Acoustics
J_2	=	Bessel function of the first order, second kind
k	=	wave number
M_{cr}	=	co rotation Mach number
p	=	far field pressure perturbations
p_n	=	normalised far field pressure, $p/(\rho_o c^2)$
r	=	distance from vortex core
r^*	=	far field observation position
R	=	half of total separation distance between vortex cores
R_o	=	radius of vortex core
Re	=	Reynolds number
t^*	=	retarded time, $(t - r^*/c)$
Y_2	=	Bessel function of the second order, second kind
Δx_{cfd}	=	spatial size of CFD cell
Δx_{caa}	=	spatial size of CAA cell
Γ_o	=	initial circulation of vortex core
Ω_k	=	angular rate of rotation of co-rotating vortex cores in the k direction
ζ_k	=	vorticity of flow in the k direction
ρ_o	=	ambient density in acoustic medium
ρ	=	far field density perturbations
λ	=	wavelength of acoustic waves
μ	=	dynamic viscosity of flow
μ_a	=	artificial dissipation

Introduction

Studies on the far field acoustic effects of low speed, coherent flow structures are important in understanding noise generation in areas such as jet noise, cavity noise and edge tones. In the absences of solid surfaces, Lighthill's acoustic theory defines the fluctuating rates of momentum as the source of sound while Powell relates the source of sound to the dynamics of vorticity.

The numerical study of the acoustics of a co-rotating vortex pair

has received much attention ([3], [5], [7]). There is a range of computational aeroacoustic issues that are fundamental to generating accurate acoustic solutions ([2], [10]).

There are numerous ways of numerically modelling the far field acoustics of low Mach number flow fields (ie. DNS, acoustic analogies, Kirchhoff's method [6], Hardin-Pope formulations [3]). Acoustic analogies have the advantage of providing a better analysis of the acoustic field by virtue of being decoupled from the flow field. Computation wise, it is also considerably less intensive than DNS.

The motivation for this study is to investigate the numerical feasibility of using Lighthill's acoustic analogy and Powell's theory of vortex sound for the simple flow configuration of a co-rotating vortex pair. Further development can lead to applying the method to investigate more complex flows such as vortex rings collisions, leap-frogging motion of vortex rings, etc.

Aeroacoustic theory

The acoustic theory developed by Lighthill [4] assumes that the far field acoustic medium is at rest. This is valid for the case of low Mach number flows. Using ρ as the fundamental acoustic variable, Lighthill derived the far field sound as

$$\frac{\partial^2 \rho}{\partial t^2} - c^2 \nabla^2 \rho = \rho_o \frac{\partial^2 u_i u_j}{\partial x_i \partial x_j}. \tag{1}$$

Powell's [9] theory of vortex sound relates the acoustic pressure to the Coriolis acceleration term, $\zeta_k \times \mathbf{V}$,

$$\frac{\partial^2 p}{\partial t^2} - c^2 \nabla^2 p = \rho_o \nabla \cdot (\zeta_k \times \mathbf{V}). \tag{2}$$

The far field acoustics of a pair of co-rotating inviscid point vortices has been studied analytically by [8]. In that case, the period of the circular motion of the two point vortices is $8\pi^2 R^2/\Gamma_o$ and the wavelength of the acoustic waves $\lambda = 52R$. The acoustic pressure contours were found to be of a quadrupolar nature. Using the method of matched asymptotic expansions, an analytical solution for the far field acoustic pressure was derived as follows,

$$p(r^*, t^*) = \frac{\rho_o \Gamma_o^4}{64\pi^3 R^4 c^4}(J_2(kr^*)\sin(2\theta + \Omega_k t) \tag{3}$$
$$-Y_2(kr^*)\cos(2\theta + \Omega_k t)).$$

Flow description

The flow field is assumed to be viscous and incompressible. The vortices of circulation strength Γ are placed a distance $2R$ apart (see Figure 1) [1]. The vorticity distribution of the vortex core is Gaussian,
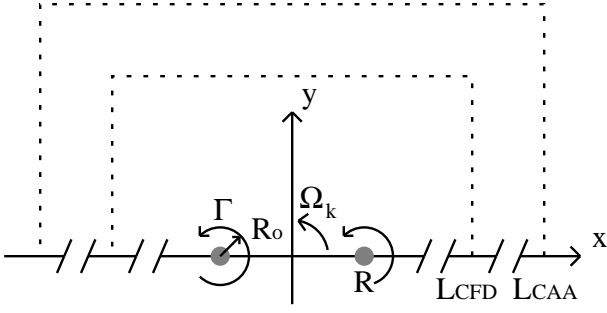
---

[1]Specifications of flow field are similar to [7]

Figure 1: Schematic diagram of flow configuration.
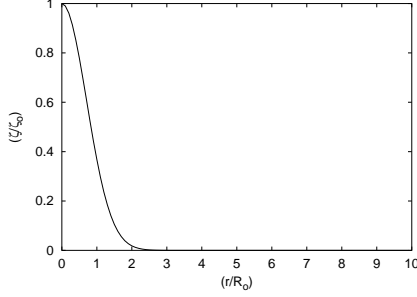

Figure 2: Vortex core vorticity profile against normalised distance.

$$\zeta_k(r,t=0) = \frac{3.57 \times 0.7\Gamma_o}{2\pi R_o^2} \exp(-1.25(-r/R_o)^2). \quad (4)$$

Computational analysis

The acoustic source formulations of [4] and [9] are evaluated using the CFD flow field simulations. CAA is used to compute far field acoustic pressures. An interpolation algorithm is used to interpolate the flow variables spatially and temporally from the CFD grid to the CAA grid.

Computational fluid dynamics

The two dimensional unsteady, viscous, incompressible flow field is modelled using the commercial finite-volume software package Fluent. The spatial convective terms in the momentum equations were discretized using the QUICK scheme. Pressure-velocity coupling was solved using the SIMPLE algorithm. The flow field was marched temporally using a second-order implicit scheme.

Numerical simulations are performed on a square $L_{cfd} \times L_{cfd}$ domain. It extends $30R$ in the x, y directions. Using the incompressibility condition, $\nabla.\mathbf{V} = 0$, the flow field is initialised as the vector sum of the velocity field of each vortex core. At the computational boundaries, the velocity field is based on the analytical solution of a single vortex of circulation, Γ_o.

Computational aeroacoustics

The inhomogeneous acoustic wave equation is rewritten as a set of first order differential equations.

$$\frac{\partial \mathbf{q}}{\partial t} + \frac{\partial \mathbf{E}}{\partial x} + \frac{\partial \mathbf{F}}{\partial y} = \mathbf{H}(x,y,t) \quad (5)$$

where

$$\mathbf{q} = \begin{vmatrix} \frac{\partial p_n}{\partial t} \\ \frac{\partial p_n}{\partial x} \\ \frac{\partial p_n}{\partial y} \end{vmatrix} \quad \mathbf{E} = \begin{vmatrix} \frac{\partial p_n}{\partial x} \\ \frac{\partial p_n}{\partial t} \\ 0 \end{vmatrix} \quad \mathbf{F} = \begin{vmatrix} \frac{\partial p_n}{\partial y} \\ 0 \\ \frac{\partial p_n}{\partial t} \end{vmatrix} \quad (6)$$

The governing equations are solved using a finite-difference formulation. The spatial terms are solved on a seven-point central difference stencil which is sixth order accurate in space. The flow is advanced in time using the standard fourth order Runge-Kutta scheme.

A second order artificial dissipation term, $\mu_a \nabla^2 \mathbf{q}$ is added to the governing equations to reduce the presence of numerical noise. This is necessary to reduce the non physical oscillations but not to unduly affect the amplitudes of the wave solution. The dissipation term is frozen during each substep of the Runge-Kutta scheme.

The computational aeroacoustic (CAA) domain extends to two wavelengths in the x, y directions ($L_{caa} = 105R$). Of interest is the fact that the CAA grid is about three times larger than the CFD grid (due to the large disparate eddy lengthscales and acoustic wavelengths). An exponential function was used model the CAA grid. A uniform near field is introduced followed by a smooth transition to the far field. Radiation boundary conditions based on [1] were adopted. A seven-point stencil creates three ghost points on the boundary region. Backward differencing was used when necessary to treat the boundary points so that sixth order accuracy was maintained.

Interpolation from CFD to CAA

Bilinear interpolation is used to interpolate flow field variables, u, v, ζ from the CFD domain to the CAA domain. The flow variables from the CFD grid is stored at every $5\Delta t_{cfd}$. A six point cubic spline was used to interpolate the acoustic field between the intervals. On the CAA domain which lies outside the CFD region, the velocity and vorticity fields were based on the values of the potential flow velocity and vorticity fields. No spatial truncation of acoustic source terms were performed.

Results and Discussion

Results are presented for the flow field for a Reynolds number based on circulation of each vortex, $\rho_o \Gamma_o / \mu = 7500$. The aspect ratio R_o/R is 0.15. The initial co-rotation Mach number $\Omega_k R/c$ is set at 0.06.

Flow simulations

The influence of spatial resolution of the flow simulations is studied by using different grid sizes ($8, 10, 14$ points across vortex core). Temporal damping is tested by choosing different time steps over the spatial grid ($\Delta t_{cfd} = 0.5s, 0.25s, 0.125s, 0.0625s$). The timewise trace of peak vorticity is used to monitor the effects of numerical dissipation. After extensive testings, for the flow simulations, the spatial grid of 12 points across vortex core and timestep, $\Delta t_{cfd} c/R = 0.2933$ were adopted.

Figure 4 shows the temporal evolution of vorticity contours at various non-dimensionalised time-frames. For the flow field, there are three different regimes (see Figure 5). Between non-dimensionaliised time units of 0 and 400, the flow field undergoes four periods of co-rotation. The flow behaviour is almost inviscid-like with the period of co-rotation similar to the case of [8]. Peak-to-peak vorticity distance is almost unity. Between tc/R of 400 and 580, the angular rotation rate decreases as the vortices move closer to each other to conserve angular momen-

tum. The final state of the flow field is a single vortex patch. Temporal trace of peak-to-peak vorticity indicates that the final 'single' vortex patch actually consists of two intertwined vortex patches. This process of merging is a direct result of flow viscosity. DNS results of [7] show three periods instead of four. This was attributed to compressibility effects in addition to flow viscosity.

Aeroacoustic simulations

The CAA grid contains 600^2 mesh points in the square domain. Resolution wise, there are approximately 30 grid points across the vortex core and far field spacing $\Delta x_{caa}/\lambda = 0.02857$. The maximum value of the local stretching is 2.07%. The time step chosen is $\Delta t_{caa}c/R = 0.00229$.

A clear distinction has to be made between the acoustic transients and the far field acoustic waves. The far field acoustic waves are sinusoidal and are of physical nature while the acoustic transients are a result of the numerical approximation to the governing equations. Previous numerical studies [5], [7] have reported on the presence of an initial high frequency component followed by the sinusoidal acoustic pressure. The former were classified as initial acoustic transients. The source of such errors may lie in the impulsively started vortex pair that generates spurious waves. As these waves propagate through the stretched region (see Figures 6 and 7), their amplitudes increase, finally leading to numerical instability.

To achieve temporal continuity in the acoustics simulations, an exponential ramping function was used to ramp the vortex cores to full strength. The ramping interval is achieved through 1600 acoustics time-steps. The corresponding values of the acoustics variables, $\mathbf{q}(x, y, t = 0)$ will form the initial conditions of the CAA simulations of the unsteady co-rotating vortex pair.

To study the effects of initial conditions, the vortex core velocity and vorticity fields were first ramped up to full strength and subsequently, held stationary. Long time integration will then result in a steady-state acoustic solution. No artificial dissipation was introduced at this stage. In both [4]'s and [9]'s formulations, the implementation of a temporal ramping function has the effect of reducing the amplitudes and frequencies of the spurious reflections of the acoustic transients (see Figures 6 and 7).

Artificial dissipation is added throughout the entire evolution of the acoustic simulations to reduce the small reflections that still persist with the new initial condition. The dissipation parameter, μ_a, is tested over the first three acoustic periods. Numerical simulations are compared with the analytical solution of [8]. The root-mean-square error is evaluated across the entire x-axis. The values of μ_a tested are $8.0, 16.0, 32.0$. The chosen value of 32.0 was found subsequently to have an RMS error of 3.248×10^{-5}.

The far field observation position is placed along the x axis at a distance $\lambda/2$. Using [9]'s theory, the far field acoustic waves show an increase in amplitude as merging occurs. Comparison of the numerical simulations with the analytical solution (Figure 7) indicates that pre-merging, the acoustic periods and amplitudes agrees reasonably well. Comparison with [7]'s results (Figure 8) reveals the suppression of the initial acoustic transients using the current method. As the vortex cores begin to merge, the acoustic pressures begin to peak. After the peak, the subsequent minor acoustic oscillations indicate unsteadiness of the flow caused by the rotation of the two intertwined vortex patches.
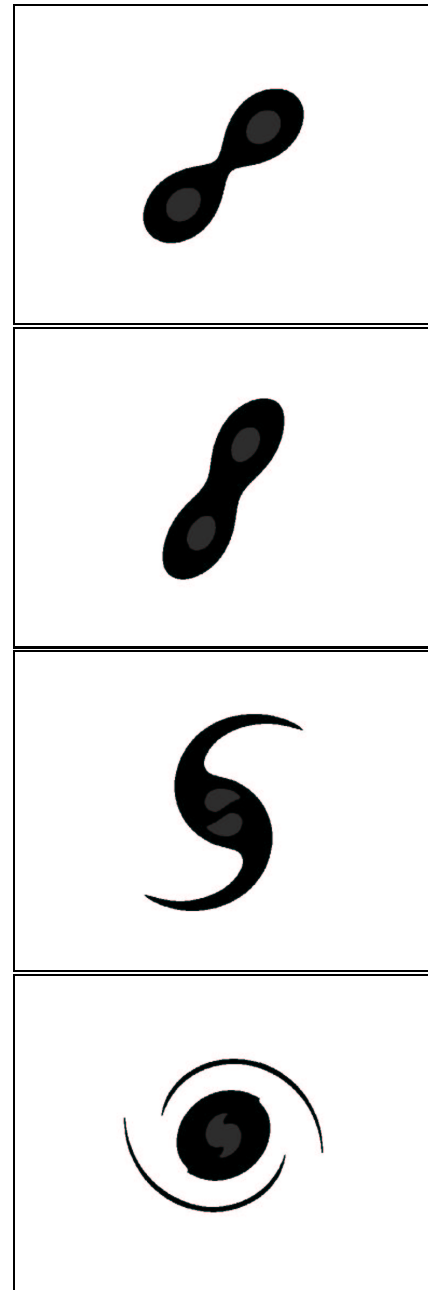
Conclusions

Figure 3: Vorticity contours at non-dimensionalised time, tc/R = $423, 470, 510, 535$. Note: outer contour is set at 1% initial peak vorticity.
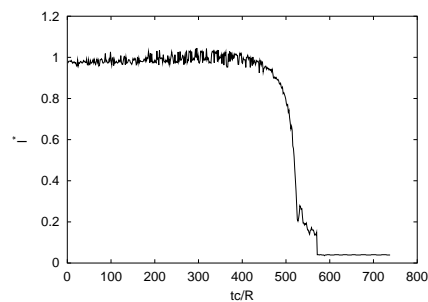

Figure 4: Trace of separation distance of peak vorticities normalised by $2R$. Note $l^* = r/(2R)$ where r is the peak-to-peak vorticity distance.
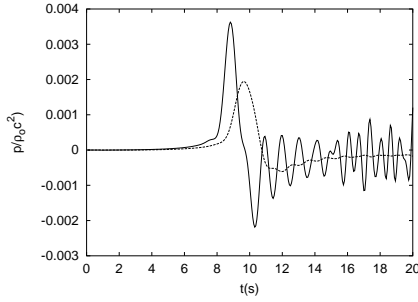
Figure 5: Trace of far field initial transient of impulsively-started — and exponentially ramped initial conditions using Lighthill's formulation at $r = \lambda/2 \cdots$.
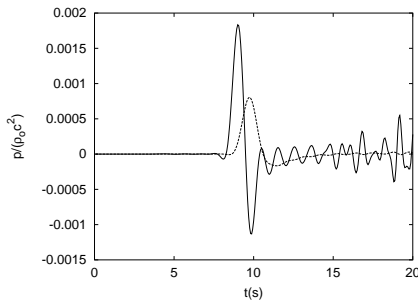

Figure 6: Trace of far field initial transient of impulsively-started — and exponentially ramped initial conditions using Powell's formulation at $r = \lambda/2 \cdots$.
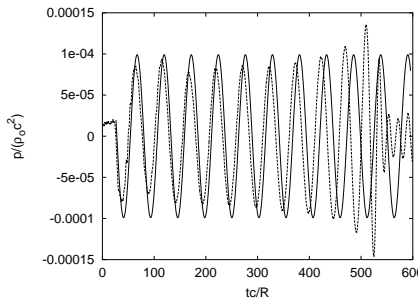

Figure 7: Far field trace of acoustic pressure at $r = \lambda/2$ along positive x-axis with [9]'s formulation $\cdots$ and analytical solution of [8] —.
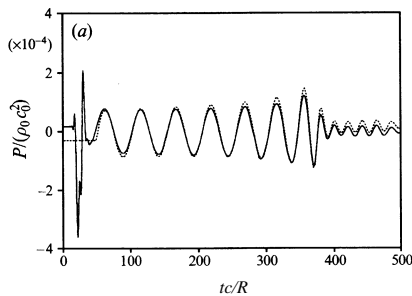

Figure 8: Far field trace of acoustic pressure at $r = \lambda/2$ along positive x-axis of [7]'s DNS results —.

The numerical application of Lighthill's acoustic analogy and Powell's theory of vortex sound is demonstrated. CFD is used to model the flow field of an incompressible, viscous co-rotating vortex pair. The flow field variables are then exported to the CAA grid which computes the far field acoustic signals. Current developments involve analysing the timewise behaviour of the source terms. Future work includes applying the numerical method to studying the acoustics of interacting coherent flow structures (ie. leap-frogging vortices and collisions of vortices).

Acknowledgements

References

[1] Bayliss, A., and Turkel, E., Radiation boundary conditions for wave-like equations, *Comm. Pure and Appl. Maths.*, **XXXIII**, 1980, 707–725.

[2] Crighton, D.G., Goals for computational aeroacoustics, *Proceedings of the 1st IMACS Symposium on Computational Acoustics*, **2**, 1986, 3–20.

[3] Ekaterinaris, J.A., New formulation of Hardin-Pope equations for aeroacoustics, *AIAA Journal*, **37**, No. 9, 1999, 1033–1039.

[4] Lighthill, M.J., On sound generated aerodynamically:I. General Theory, *Proceedings of the Royal Society of London Series A: Mathematical and Physical Sciences*, **211**, 1952, 564–587.

[5] Lee, D.J. and Koo, S.O., Numerical study of sound generation due to a spinning vortex pair, *AIAA Journal*, **33**, 1995, 20–26.

[6] Lyrintzris, A.S., Review: the use of Kirchhoff's method in computational aeroacoustics, *Journal of Fluids Engineering*, **116**, No 4, 1994, 665–676.

[7] Mitchell, B.E., Lele, S.K., and Moin, P., Direct computation of the sound from a compressible co-rotating vortex pair, *Journal of Fluid Mechanics*, **285**, 1995, 181–202.

[8] Müller, E.-A, and Obermeier, F., The spinning vortices as a source of sound, *AGARD-CP22* , 1967, 22.1–22.8.

[9] Powell, A., Theory of vortex sound, *Journal of the Acoustical Society of America*, **36**, 1964, 177–195.

[10] Tam, C.K.W., Computational aeroacoustics: issues and methods, *AIAA Journal*, **33**, No. 10, 1995, 1788–1796.